Science AAAS

www.sciencemag.org/cgi/content/full/1182840/DC1

# Supporting Online Material for

## Universality in Three- and Four-Body Bound States of Ultracold Atoms

Scott E. Pollack,* Daniel Dries, Randall G. Hulet

*To whom correspondence should be addressed. E-mail: scott.pollack@rice.edu

Published 19 November 2009 on *Science* Express
DOI: 10.1126/science.1182840

**This PDF file includes:**

Materials and Methods
Figs. S1 to S4
References

Supporting Online Material for

# Universality in Three- and Four-Body Bound States of Ultra-cold Atoms

S. E. Pollack, D. Dries, R. G. Hulet

# Materials and Methods

A set of non-Helmholtz coils are used to add or subtract additional axial confinement in the hybrid magnetic plus optical dipole trap used in the experiment. The radial trapping frequency $\omega_r$ is determined from atom loss by parametric excitation, and the axial trapping frequency $\omega_z$ is determined from collective dipole oscillations.

## Determination of Scattering Length

The *s*-wave scattering length $a$ is controlled via a magnetic Feshbach resonance (*S1*). We extract $a$ (for $a > 0$) as a function of magnetic field $B$ from the axial size of a Bose-Einstein condensate (*S2*). The measured functional form of $a$ vs. $B$ is well described by a Feshbach resonance fit $a(B) = a_{BG}[1 + \Delta/(B - B_\infty)]$, where the values $a_{BG} = -24.5^{+3.0}_{-0.2}\, a_0$, $\Delta = 192.3(3)$ G, and $B_\infty = 736.8(2)$ G were previously reported (*S2*). The standard deviation of the residuals from the Feshbach resonance fit is 15% for $a < 10^3\, a_0$ and 30% for $a > 10^3\, a_0$ (Fig. S2).

To repeatably achieve very large values of $a$ it is necessary to have both high field stability and accurate knowledge of the location of $B_\infty$. We determine the shot-to-shot stability and calibration of the magnetic field from radio frequency spectroscopy on the $|1, 1\rangle \rightarrow |2, 2\rangle$ transition. We have improved the control of the current in the coils that provide the magnetic bias field in our experiment such that a Lorentzian characterizing the shot-to-shot field stability has a full width at half maximum of 115 kHz, corresponding to 42 mG at a bias field of 717 G (Fig. S3C). With this improved field stability we have increased the precision in the determination of the resonance location to $B_\infty = 736.97(7)$ G. The uncertainty in $B_\infty$ is dominated by systematic uncertainty in the extracted values of $a$ from the measured axial sizes (*S2*). The fractional uncertainty in the determination of $a$ is given by $\delta a/a = \delta B/(B - B_\infty) \approx 1.5 \times 10^{-5}\, a/a_0$, where $\delta B$ is dominated by the uncertainty in $B_\infty$.

Since we have only measured $a$ for $a > 0$, we have no direct knowledge of $a < 0$. However, a coupled-channels calculation (*S3*) agrees with the Feshbach resonance fit to within 10% over the range of $10 < a/a_0 < 4 \times 10^4$ (Fig. S3) which gives us confidence that the Feshbach resonance fit is equally reliable on the $a < 0$ side of the resonance.

## Determination of the Loss Coefficients

Extraction of $L_3$ and $L_4$ from the measured atom number loss curves $N(t)$ requires the evaluation of the spatially-averaged moments of the density distribution $\langle n^2\rangle$ and $\langle n^3\rangle$. By comparing the measured distributions with a Thomas-Fermi inverted parabola in the case of a pure Bose-Einstein condensate, we find to a good approximation that the distributions remain in thermal equilibrium throughout the decay process. For a condensate, the axial Thomas-Fermi radius is $R = (15\hbar^2\omega_r^2 Na/m^2\omega_z^4)^{1/5}$, the peak density is $n_0 = (15N\omega_r^2)/(8\pi R^3\omega_z^2)$, and $\langle n^2\rangle = \gamma^{2/5}N^{4/5}$, where $\gamma = (25\,m^6\omega_r^4\omega_z^2)/(6272\sqrt{42}\,\pi^5\hbar^6 a^3)$. The observed decay fits well to a purely three-body loss process for a condensate, so we neglect $L_4$ in this case. Since we are not explicitly fitting for $L_4$, four-body effects if present may lead to an increase in the extracted loss rate $L_3$ (*S4*). The decay is then described by

$$\frac{1}{N}\frac{dN}{dt} = -\frac{g^{(3)}}{3!}L_3\gamma^{2/5}N^{4/5}, \tag{S1}$$

which has the solution

$$N(t) = \frac{N_0}{\left(1 + \frac{4}{5}\frac{g^{(3)}L_3}{3!}\gamma^{2/5}N_0^{4/5}t\right)^{5/4}}. \tag{S2}$$

A thermal gas is well described by a cylindrically-symmetric Gaussian where $\langle n^2\rangle = n_p^2/\sqrt{27}$, $\langle n^3\rangle = n_p^3/8$, and the peak density is $n_p = N(\omega_z/\omega_r)[m\omega_r^2/2\pi k_B T]^{3/2}$. Heating due to recombination is expected to become important when $\epsilon \lesssim U$ (*S5*). However, there is no appreciable change observed in the Gaussian width during the decay even though the loss mechanism preferentially targets atoms at higher densities. This may be due to a lack of rethermalization during the decay (*S6*). We find that both $L_3$ and $L_4$ contribute to the loss for the thermal gas. Since we have not found a closed-form solution to Eq. 1, we instead use the following implicit solution to extract $L_3$ and $L_4$:

$$t = \frac{3\sqrt{3}}{2n_p^2L_3}\left[\left(\frac{N_0}{N}\right)^2 - 1\right] + \frac{27L_4}{8n_pL_3^2}\left(1 - \frac{N_0}{N}\right) - \frac{81\sqrt{3}L_4^2}{64L_3^3}\log\left[\left(\frac{N}{N_0}\right)\frac{8\sqrt{3}L_3 + 9L_4n_p}{8\sqrt{3}L_3 + 9L_4n_p(N_0/N)}\right], \tag{S3}$$

where we have assumed $g^{(3)} = 3!$ and $g^{(4)} = 4!$ for a non-condensed gas.

In Fig. 1 the vertical error bars correspond to the range in $L_3$ for which the $\chi^2$ of the fit to Eq. S3 increases by one, while simultaneously adjusting $L_4$ and $N_0$ to minimize $\chi^2$. Systematic uncertainties in $\omega_r$, $\omega_z$, $N$, and $T$, which are not included in these error bars, contribute as much as a factor of 2 in the uncertainty of $L_3$. The representative horizontal error bars are due to shot-to-shot variation in the magnetic field and the determination of $a$ from the Feshbach resonance fit. Background loss limits the sensitivity of the measurement to $L_3 > 2(1)\times10^{-28}$ cm$^6$/s. The error bars in Fig. 2 are similarly determined.

## Comparing with Theory

The universal theory (*S7*) describing Efimov physics predicts that the three-body loss rate coefficient is described by $L_3(a) = 3C(a)\hbar a^4/m$ where $C(a)$ is a logarithmically periodic modulation. The following expression describes this modulation:

$$C(a) = \begin{cases} \dfrac{4590 \sinh(2\eta^-)}{\sin^2(s_0 \ln(a/a^-)) + \sinh^2 \eta^-} & (a < 0), \\ 67.12 e^{-2\eta^+}\left[\sin^2(s_0 \ln(a/a^+)) + \sinh^2 \eta^+\right] + 16.84(1 - e^{-4\eta^+}) & (a > 0), \end{cases} \tag{S4}$$

where the first and second terms for $a > 0$ account for coupling to weakly- and deeply-bound dimer states, respectively (*S7,S8*). The value $a^-$ denotes the resonance location when the energy of the Efimov trimer is degenerate with the free atom continuum, and the value $a^+$ is the location of a recombination minimum (*S9*). This expression is log-periodic with $C(e^{\pi/s_0}a) = C(a)$, where the universal parameter $s_0 = 1.00624$ is known from theory (*S7, S10*).

The four-body loss coefficient $L_4$ is predicted to have a similar form to that of $L_3$:

$$L_4(a, a^T) = 4\, C_4 \frac{\hbar |a|^7}{m} \frac{\sinh(2\eta^-)}{\sin^2(s_0 \ln(a/a^T)) + \sinh^2 \eta^-} \qquad (a < 0), \tag{S5}$$

where $C_4$ is a theoretically undetermined universal constant (*S11*). Eq. S5 is phenomenologically derived from the theory of Ref. S11 (*S12*). We find that $C_4 = 16(8) \times 10^4$ in the region $1000 < -a/a_0 < 2500$, assuming that $\eta^- = 0.13$, as for the three-body resonance. In Fig. 2 we plot $\frac{1}{2}\{L_4(a, 0.90\, a_1^-) + L_4(a, 0.43\, a_1^-)\}$ where we have replaced $a^T$ with the predicted locations of the two tetramer states linked to the first trimer state (*S4, S11*).

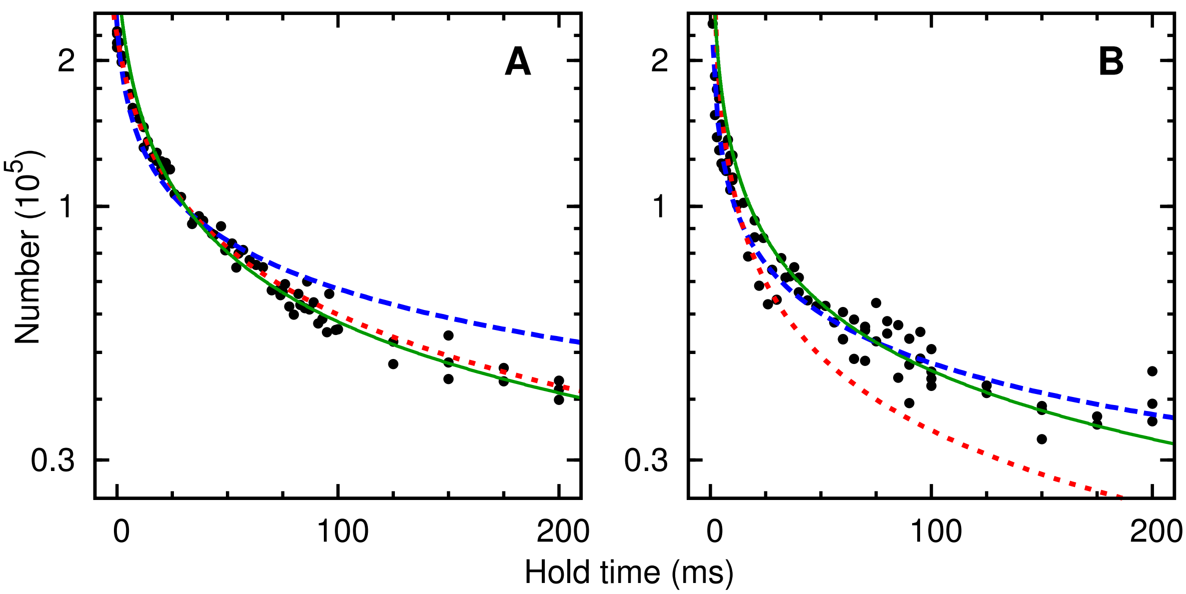


**Fig. S1.** Loss dynamics at two values of $a < 0$ for a thermal gas. The dots are data. The dotted red line is a fit of the data to the solution of Eq. 1 with only three-body loss accounted for, the dashed blue line is the fit when only four-body loss is included, and the solid green line is a fit accounting for both effects (Eq. S3). (**A**) $a = -1800\,a_0$, where three-body losses dominate; (**B**) $a = -3300\,a_0$, near $a^T_{2,1}$ where four-body losses dominate.

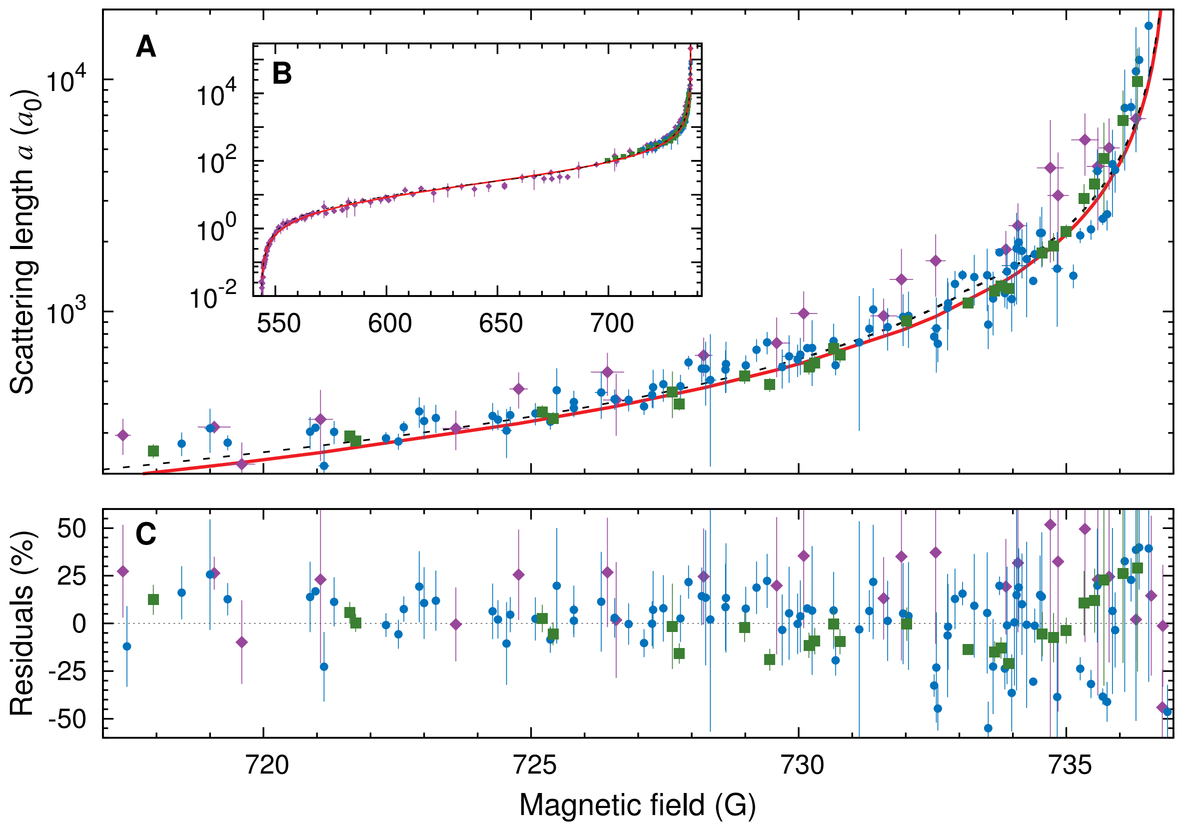


**Fig. S2.** (**A**) $a$ extracted from the axial size of Bose-Einstein condensates as a function of magnetic field. Results of a coupled-channels calculation are shown by the solid red line. The dashed black line is the Feshbach resonance fit. (♦) Data previously reported with trapping frequencies $\omega_r = (2\pi)\,193\,\mathrm{Hz}$ and $\omega_z = (2\pi)\,3\,\mathrm{Hz}$ (*S2*). Data with $\omega_r = (2\pi)\,236\,\mathrm{Hz}$ and $\omega_z = (2\pi)\,4.6\,\mathrm{Hz}$ (●) or $\omega_z = (2\pi)\,16\,\mathrm{Hz}$ (■). Beyond mean field effects become important when $n_0 a^3 \gtrsim 0.1$ (*S13*). We apply a mean field correction for data with $0.1 < n_0 a^3 < 1$, and omit data with $n_0 a^3 > 1$ in the Feshbach resonance fit (*S2*). (**B**) Full range of data spanning 7 decades in $a$. (**C**) Fractional residuals of the extracted values of $a$ from the Feshbach resonance fit.

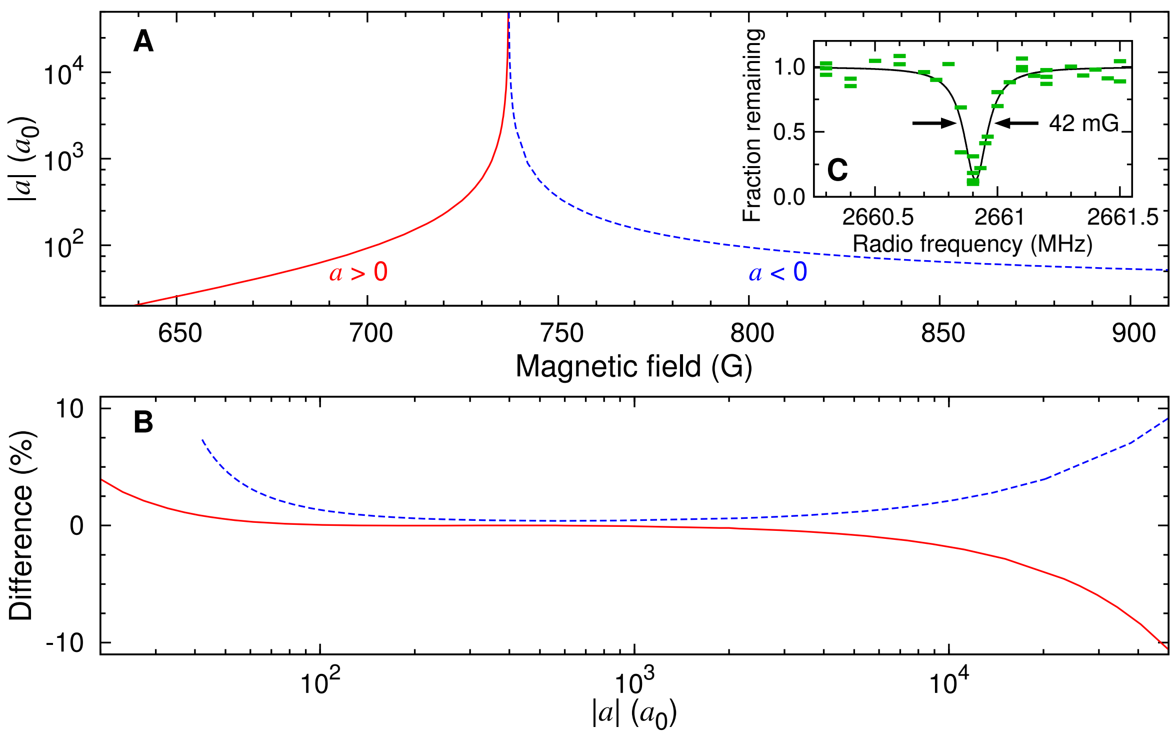


**Fig. S3.** (**A**) $a$ vs. magnetic field from a coupled-channels calculation. (**B**) Fractional difference between the coupled-channels calculation and the Feshbach resonance fit used to determine $a$ (solid red line $a > 0$, dashed blue line $a < 0$). (**C**) Radio frequency spectroscopy signal at 717 G showing a full width at half maximum of 115 kHz.

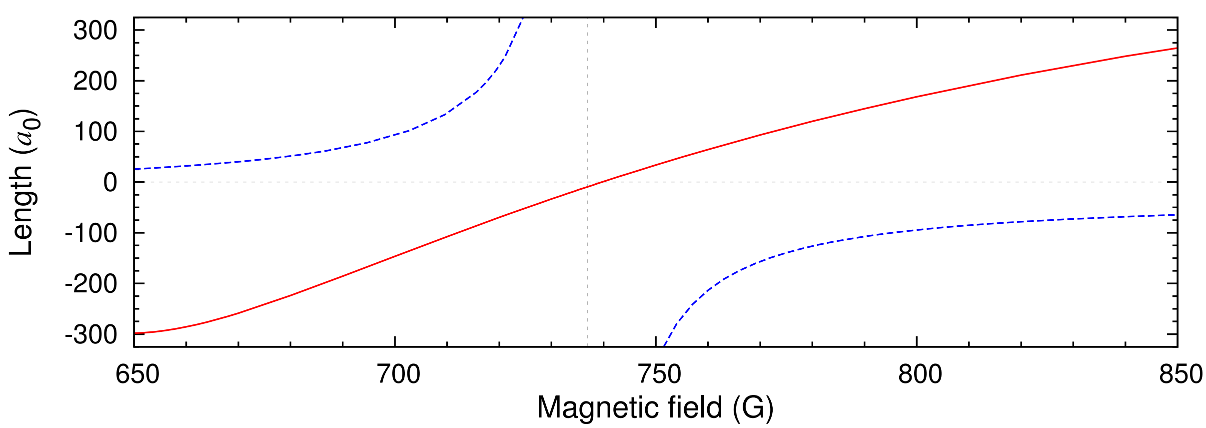


**Fig. S4.** The effective range $R_e$ (solid red) and scattering length $a$ (dashed blue) vs. magnetic field, extracted from a coupled-channels calculation through a low energy expansion $k \cot \delta = -1/a + R_e k^2/2$, where $\delta$ is the scattering phase shift (*S1*). The dotted vertical line is the location of $B_\infty$.

# References

S1. C. Chin, R. Grimm, P. Julienne, E. Tiesinga, *arXiv:0812.1496v2* (2009).

S2. S. E. Pollack *et al.*, *Phys. Rev. Lett.* **102**, 090402 (2009).

S3. M. Houbiers *et al.*, *Phys. Rev. A* **56**, 4864 (1997).

S4. J. von Stecher, J. P. D'Incao, C. H. Greene, *Nature Phys.* **5**, 417 (2009).

S5. T. Weber, J. Herbig, M. Mark, H.-C. Nägerl, R. Grimm, *Phys. Rev. Lett.* **91**, 123201 (2003).

S6. F. Ferlaino *et al.*, *Phys. Rev. Lett.* **102**, 140401 (2009).

S7. For a review, see E. Braaten, H.-W. Hammer, *Phys. Rep.* **428**, 259 (2006).

S8. B. D. Esry, C. H. Greene, J. P. Burke, *Phys. Rev. Lett.* **83**, 1751 (1999).

S9. E. Nielsen, J. H. Macek, *Phys. Rev. Lett.* **83**, 1566 (1999).

S10. V. Efimov, *Sov. J. Nucl. Phys.* **12**, 589 (1971).

S11. N. P. Mehta, S. T. Rittenhouse, J. P. D'Incao, J. von Stecher, C. H. Greene, *Phys. Rev. Lett.* **103**, 153201 (2009).

S12. C. H. Greene, private communication.

S13. T. D. Lee, K. Huang, C. N. Yang, *Phys. Rev.* **106**, 1135 (1957).